1521-0103/375/2/308–316$35.00
THE JOURNAL OF PHARMACOLOGY AND EXPERIMENTAL THERAPEUTICS

https://doi.org/10.1124/jpet.120.265876
J Pharmacol Exp Ther 375:308–316, November 2020

The Journal of PHARMACOLOGY And Experimental Therapeutics

High-Density Lipoprotein Mimetic Peptide 4F Efficiently Crosses the Blood-Brain Barrier and Modulates Amyloid-β Distribution between Brain and Plasma

Suresh K. Swaminathan,[1] Andrew L. Zhou,[1] Kristen M. Ahlschwede, Geoffry L. Curran, Val J. Lowe, Ling Li, and Karunya K. Kandimalla

Department of Pharmaceutics and Brain Barriers Research Center (S.K.S., A.L.Z., K.M.A., K.K.K.) and Department of Experimental and Clinical Pharmacology (L.L.), University of Minnesota, College of Pharmacy, Minneapolis, Minnesota; Department of Pharmaceutical Sciences, College of Pharmacy, Rosalind Franklin University of Medicine and Science, North Chicago, Illinois (K.M.A.); and Departments of Radiology (G.L.C., V.J.L.) and Neurology (G.L.C.), Mayo Clinic, College of Medicine, Rochester, Minnesota

Received March 3, 2020; accepted July 24, 2020

ABSTRACT

Treatments to elevate high-density lipoprotein (HDL) levels in plasma have decreased cerebrovascular amyloid -β (Aβ) deposition and mitigated cognitive decline in Alzheimer disease (AD) transgenic mice. Since the major protein component of HDL particles, apolipoprotein A-I (ApoA-I), has very low permeability at the blood-brain barrier (BBB), we investigated 4F, an 18-amino-acid ApoA-I/HDL mimetic peptide, as a therapeutic alternative. Specifically, we examined the BBB permeability of 4F and its effects on [^{125}I]Aβ trafficking from brain to blood and from blood to brain. After systemic injection in mice, the BBB permeability of [^{125}I]4F, estimated as the permeability–surface area (PS) product, ranged between 2 and 5 $\times$ 10^{-6} ml/g per second in various brain regions. The PS products of [^{125}I]4F were ~1000-fold higher compared with those determined for [^{125}I]ApoA-I. Moreover, systemic infusion with 4F increased the brain efflux of intracerebrally injected [^{125}I]Aβ42. Conversely, 4F infusion decreased the brain influx of systemically injected [^{125}I]Aβ42. Interestingly, 4F did not significantly alter the brain influx of [^{125}I]Aβ40. To corroborate the in vivo findings, we evaluated the effects of 4F on [^{125}I]Aβ42 transcytosis across polarized human BBB endothelial cell (hCMEC/D3) monolayers. Treatment with 4F increased the abluminal-to-luminal flux and decreased the luminal-to-abluminal flux of [^{125}I]Aβ42 across the hCMEC/D3 monolayers. Additionally, 4F decreased the endothelial accumulation of fluorescein-labeled Aβ42 in the hCMEC/D3 monolayers. These findings provide a mechanistic interpretation for the reductions in brain Aβ burden reported in AD mice after oral 4F administration, which represents a novel strategy for treating AD and cerebral amyloid angiopathy.

SIGNIFICANCE STATEMENT

The brain permeability of the ApoA-I mimetic peptide 4F was estimated to be ~1000-fold greater than ApoA-I after systemic injection of radiolabeled peptide/protein in mice. Further, 4F treatment increased the brain efflux of amyloid -β and also decreased its brain influx, as evaluated in mice and in blood-brain barrier cell monolayers. Thus, 4F represents a potential therapeutic strategy to mitigate brain amyloid accumulation in cerebral amyloid angiopathy and Alzheimer disease.

Introduction

Toxic amyloid-β (Aβ) peptides generated in the brain accumulate as senile plaques in the brain parenchyma, constituting one of the pathologic hallmarks of Alzheimer disease (AD). In around half of individuals over 60 years of age and in 95% of patients with AD, Aβ also accumulates in the cerebral vasculature, which culminates in cerebral amyloid angiopathy (CAA) (Herzig et al., 2006; Charidimou et al., 2012; Yamada and Naiki, 2012). CAA triggers cerebrovascular inflammation and represents the major cause of intracerebral hemorrhages, which lead to rapid decline in cognitive and neurologic functions in older subjects with and without AD pathology (Viswanathan and Greenberg, 2011; Charidimou et al., 2012). The two major Aβ isoforms associated with CAA and AD are Aβ40 and Aβ42, respectively, which differ by the presence of two additional amino acids on the C-terminus. Aβ40 is considered to be the

This work was supported by the Minnesota Partnership for Biotechnology and Medical Genomics [Grant RF1-00056030] and by National Institutes of Health National Institute on Aging [Grant RF1-AG058081] and [Grant R21-AG056025].
[1]S.K.S. and A.L.Z. contributed equally to this work.
https://doi.org/10.1124/jpet.120.265876.

ABBREVIATIONS: Aβ, amyloid-β; ABCA1, ATP-binding cassette transporter A1; AD, Alzheimer disease; A-L, abluminal-to-luminal; ApoA-I, apolipoprotein A-I; AUC, area under the curve; BBB, blood-brain barrier; CAA, cerebral amyloid angiopathy; CVD, cardiovascular disease; F-Aβ40, fluorescein-labeled Aβ40; F-Aβ42, fluorescein-labeled Aβ42; hCMEC/D3, human cerebral microvascular endothelial cell; HDL, high-density lipoprotein; L-A, luminal-to-abluminal; LRP1, low-density lipoprotein receptor-related protein 1; PS, permeability–surface area product; SR-B1, scavenger receptor class B type 1; TCA, trichloroacetic acid.

more vasculotropic isoform, whereas Aβ42 is considered to be more neurotoxic and amyloidogenic (Qi and Ma, 2017). The blood-brain barrier (BBB) maintains a dynamic equilibrium between brain and plasma Aβ pools. Along with perivascular drainage, the BBB participates in Aβ clearance from the brain. Disruption of these spatially coordinated Aβ clearance portals is believed to cause anomalous Aβ accumulation in the brain parenchyma and in the cerebral vasculature (Michaud et al., 2013a,b). The use of pharmacological agents to remodel Aβ trafficking mechanisms at the BBB and promote Aβ clearance from the brain could therefore improve vascular health and mitigate cognitive decline in CAA and AD.

It is well established that high-density lipoprotein (HDL) particles in plasma help to mitigate the formation of atherosclerotic plaques, thereby protecting from cardiovascular disease (CVD) (Assmann and Gotto, 2004). Emerging evidence also suggests that HDL is important for cerebrovascular and neurobiological functions (Hottman et al., 2014; Button et al., 2019). The major protein constituent of HDL particles in the periphery, apolipoprotein A-I (ApoA-I), was shown to mitigate age-related cognitive decline in AD transgenic mice by us (Lewis et al., 2010) and others (Lefterov et al., 2010). These two studies established that ApoA-I overexpression reduces cerebrovascular Aβ deposition (CAA) and attenuates Aβ-associated neuroinflammation (Lewis et al., 2010), whereas ApoA-I deletion exacerbates CAA in the AD transgenic mice (Lefterov et al., 2010). Intriguingly, genetic manipulation of ApoA-I expression did not alter parenchymal Aβ deposition (Fagan et al., 2004; Lefterov et al., 2010; Lewis et al., 2010). Recently, we reported that radioiodinated ApoA-I displays very low brain permeability in Sprague-Dawley rats after systemic injection (Zhou et al., 2019). Since ApoA-I is almost exclusively expressed in the periphery, the absence of effects on parenchymal Aβ deposition could potentially be attributed to the low brain permeability of ApoA-I.

Despite the well documented cardio-, neuro-, and vasoprotective effects of ApoA-I, therapeutic applications are limited by its poor oral bioavailability, high manufacturing costs, and low brain permeability. To address these limitations, small peptides that mimic ApoA-I/HDL function have been developed (Navab et al., 2010). The most notable of these HDL mimetics is the 18-amino-acid peptide "4F," which contains four phenylalanine residues (Ac-DWFKA-FYDKVAEKFKEAF-NH_2) and was designed to mimic the amphipathic α-helix motif present in ApoA-I, which is important for its biologic activity (Anantharamaiah et al., 2007). Oral administration of 4F was shown to reduce atherosclerotic lesions and plaque inflammation in a diabetes mouse model (Morgantini et al., 2010). Treatment with 4F was also shown to decrease cerebrovascular inflammation and improve cognitive function in a mouse model of atherosclerosis (Buga et al., 2006). Moreover, oral administration of 4F together with a statin drug reduced Aβ deposition in the brain parenchyma, ameliorated Aβ-associated neuroinflammation, and improved cognitive function in an AD transgenic mouse model (Handattu et al., 2009).

These literature reports suggest that 4F could potentially be employed as a therapeutic agent to mitigate sporadic CAA- and AD-related neurovascular pathologies. However, the brain penetrance of 4F has not been established, and the mechanisms by which 4F influences parenchymal and cerebrovascular Aβ deposition are poorly understood. Here, we assessed the permeability of radioiodinated 4F versus ApoA-I at various brain regions after systemic injection in mice. Additionally, we examined the effects of 4F on both the brain efflux and brain influx of radioiodinated Aβ peptides. The in vivo findings were further supported by complementary studies conducted in BBB cell monolayers.

Materials and Methods

Animals. Wild-type mice (B6SJLF1/J) were bred in-house at the Mayo Clinic animal facilities. Animals were raised with food and water ad libitum with 12-hour light/dark cycles. Animal studies were carried out in accordance with the guide for the care and use of laboratory animals provided by the National Institutes of Health. All protocols were approved by the Mayo Clinic Institutional Animal Care and Use Committee. All studies were conducted using female mice between 8 and 12 months of age and weighing approximately 30 g.

Radioiodination of 4F, ApoA-I, and Aβ Peptides. The following peptides/proteins were labeled with ^{125}I (PerkinElmer Life and Analytical Sciences, Boston, MA) using the chloramine-T reaction as described previously (Poduslo et al., 2001; Jaruszewski et al., 2014): D-4F peptide [American Peptide Company (now Bachem), Sunnyvale, CA], human serum-derived ApoA-I (EMD Millipore, Burlington, MA), and Aβ42 and Aβ40 peptides (custom synthesized by AAPPTec, Louisville, KY, or Mayo Clinic proteomics core facility). The unconjugated ^{125}I was removed by dialysis overnight in PBS, and the purity of the radiolabeled proteins was determined by trichloroacetic acid (TCA) precipitation as described previously (Kandimalla et al., 2007). The specific activity of labeled Aβ peptides was determined to be 40 μCi/μg.

Brain Influx of [^{125}I]4F Versus [^{125}I]ApoA-I after Systemic Injection. These assays were conducted as described in our previous publications (Swaminathan et al., 2018). Briefly, mice were anesthetized under a mixture of isoflurane (1.5%) and oxygen (4 l/min) and then catheterized at the femoral vein and artery (n = 4). A bolus of [^{125}I]4F (100 μCi; 11 nmol) or [^{125}I]ApoA-I (100 μCi; 0.88 nmol) was injected into the femoral vein, and then 20-μl blood samples were collected from the femoral artery at 0.25, 1, 3, 5, 10, and 15 minutes using heparinized capillary tubes. The blood samples were diluted with saline and centrifuged to separate the plasma. The [^{125}I]4F or [^{125}I]ApoA-I in plasma was precipitated by using TCA and was centrifuged to collect the pellet. Total ^{125}I radioactivity counts in the pellet, corresponding to intact peptide/protein, were measured using a gamma counter (Cobra II; Amersham Biosciences, Piscataway, NJ). Immediately after the final sampling event, the mice were euthanized by transcardial perfusion with excess PBS to flush the remaining radioactivity from the vasculature. Individual brain regions (cortex, caudate putamen, hippocampus, thalamus, brain stem, and cerebellum) were dissected and assayed for ^{125}I radioactivity using a gamma counter.

The influx of [^{125}I]4F and [^{125}I]ApoA-I at each brain region was assessed as the permeability–surface area (PS) product. The PS product (milliliter per gram per second) at each brain region was determined using the equation

$$PS = \frac{q(t)}{\int_0^t C_p dt}$$

where $q(t)$ is the extravascular amount of [^{125}I]4F or [^{125}I]ApoA-I in the brain region per gram of tissue (μCi/g) at the end of the experiment, and $\int_0^t C_p dt$ is the area under the plasma concentration versus time profile (minute × microcurie per milliliter) from 0 to 15 minutes, calculated using the linear-trapezoidal method.

Impact of 4F on the Brain-To-Blood Efflux of [^{125}I]Aβ42. Mice were anesthetized as described above, and the left internal carotid artery was catheterized. Immediately afterward, mice were mounted on a stereotaxic apparatus. The skin above the skull was cut open, and sutures were exposed. As per the accurate stereotaxic coordinates,

a small hole was drilled into the skull directly above the hippocampus. The animals were infused over 60 minutes with or without 2 mg (0.9 μmol) of 4F peptide dissolved in 200 μl of saline (n = 3 each group) via the left internal carotid artery, which supplies blood directly to the left hemisphere and thereby allows for greater 4F exposure to the BBB. At the end of the infusion, the mice were injected with [^{125}I]Aβ42 (0.7 μCi) dissolved in PBS (1 μl) directly into the right hippocampus. After 40 minutes post–Aβ injection, the animals were transcardially perfused with excess PBS. Brain hemispheres were dissected and assayed for ^{125}I radioactivity using a gamma counter. The measured brain radioactivity per gram of tissue was normalized to the radioactivity measured at the site of injection using the following equation:

$$Brain - to - Blood\ Efflux = \frac{Radioactivity\ per\ gram\ of\ brain\ tissue\ \left(\frac{\mu Ci}{g}\right)}{Radioactivity\ at\ the\ injection\ site\ \left(\frac{\mu Ci}{g}\right)}.$$

Impact of 4F on the Blood-to-Brain Influx of [^{125}I]Aβ42 and [^{125}I]Aβ40. These assays were conducted as described in our previous publications (Swaminathan et al., 2018). Briefly, mice were anesthetized, and the femoral vein, femoral artery, and left internal carotid artery were catheterized. The animals were then infused with saline (200 μl) with or without 2 mg (0.9 μmol) of 4F peptide via the left internal carotid artery over a period of 60 minutes. After this, the animals were bolus-injected with 100 μCi of [^{125}I]Aβ42 or [^{125}I]Aβ40 into the femoral vein (n = 3 each group). Blood samples of 20 μl were collected from the femoral artery at 0.25, 1, 3, 5, 10, and 15 minutes post–Aβ injection. After separating the plasma, the intact [^{125}I]Aβ42 or [^{125}I]Aβ40 in plasma was precipitated using TCA and then centrifuged. Total ^{125}I radioactivity counts in the pellet were measured using a gamma counter. Immediately after the final sampling event, the animals were transcardially perfused with PBS, the brain regions were dissected, and the ^{125}I radioactivity was measured by using a gamma counter. The PS products for [^{125}I]Aβ42 and [^{125}I]Aβ40 at the hippocampus and the left hemisphere were determined as described above for [^{125}I]4F.

Impact of 4F on [^{125}I]Aβ42 and [^{125}I]Aβ40 Plasma Pharmacokinetics. The [^{125}I]Aβ42 and [^{125}I]Aβ40 plasma concentration versus time data from 0 to 15 minutes were evaluated by noncompartmental analysis using Phoenix WinNonlin (Certara). Parameters of interest included the area under the concentration versus time profile from 0 to 15 minutes (AUC_{0-t}; minute × microcurie per milliliter) and the terminal clearance (milliliter per minute).

Cell Culture. The immortalized human cerebral microvascular endothelial cell line (hCMEC/D3) was generously provided by Perrie-Oliver Couraud, Institut Cochin, France (Weksler et al., 2013). The cells were grown at 37°C under 5% CO_2 atmosphere on rat tail collagen (Corning, Corning, NY)-coated cell culture–grade flasks (Corning) using endothelial basal media-2 (Lonza, Walkersville, MD) supplemented with 5% FBS (Atlanta Biologicals, Flowery Branch, GA), 1% penicillin-streptomycin (Corning), 1.4 μM hydrocortisone (Sigma-Aldrich, St Louis, MO), ascorbic acid (5 μg/ml; Sigma-Aldrich), 1% chemically defined lipid concentrate (Life Technologies, Grand Island, NY), 10 mM HEPES, and 1 ng/ml basic fibroblast growth factor (Peprotech, Rocky Hill, NJ). Cells in passages 27–35 were used in the experiments.

Impact of 4F on the Abluminal-to-Luminal Versus Luminal-to-Abluminal Flux of Radioiodinated Aβ Across BBB Cell Monolayers. These experiments were performed as described in our previous publications (Agyare et al., 2013). Briefly, the hCMEC/D3 cells were cultured on 12-mm Transwell inserts with 0.4-μm pores (Corning) until a continuous monolayer was formed. The monolayer integrity was verified by measuring the transendothelial electrical resistance. Experiments were conducted when transendothelial electrical resistance values ranged between 80 and 120 Ω/cm^2. The evening before the experiment, the growth medium containing 5% FBS and 10 mM HEPES was replaced with growth medium containing 1% FBS and 20 mM HEPES. To investigate abluminal-to-luminal (A-L) transport, cells were pretreated with or without 4F (10 μg/ml) on the abluminal side for 60 minutes at 37°C (n = 4 in each group). Without removing 4F, [^{125}I]Aβ42 (10 μCi/ml) was then spiked into the abluminal medium. The luminal medium was then sampled (20 μl) at 10, 20, 30, 45, 60, and 90 minutes post–Aβ addition, and the ^{125}I radioactivity was measured using a gamma counter. Similar studies were conducted to investigate luminal-to-abluminal (L-A) transport, with 4F preincubation and [^{125}I]Aβ42 addition occurring on the luminal side, followed by sampling from the abluminal side. The cumulative amount of radioactivity reaching the contralateral side was plotted against time. The slope obtained after linear regression of the linear region of the curve, in which unidirectional transfer is assumed, was divided by the surface area of the Transwell insert (1.12 cm^2) to calculate [^{125}I]Aβ42 flux across the monolayer.

Impact of 4F on the Accumulation of Fluorescein-Labeled Aβ42 and Aβ40 in BBB Cell Monolayers. For flow cytometry studies, hCMEC/D3 cells were cultured on six-well plates (Corning) until a continuous monolayer was formed. The evening before the experiment, the growth medium containing 5% FBS was replaced with growth medium containing 1% FBS. Cells were pretreated with or without 4F (10 μg/ml) for 60 minutes at 37°C (n = 3 in each group). After this, fluorescein-labeled Aβ42 (F-Aβ42) or F-Aβ40 (synthesized by the Mayo Clinic proteomics core facility) was spiked into the media (1.5 μg/ml) and then further incubated for 60 minutes. Cells were washed three times with ice-cold PBS, trypsinized, and then resuspended in PBS followed by 1:1 dilution with 4% paraformaldehyde on ice. Cellular uptake of the fluorescence signal was measured using LSR-II Fortessa flow cytometry equipped with a 20-mW (488 nm) laser (BD Biosciences, San Jose, CA). Data analysis was performed using FlowJo software (TreeStar, Inc., San Carlos, CA).

For confocal microscopy studies, hCMEC/D3 cells were cultured on 35-mm coverslip bottom dishes (MatTek, Ashland, MA) until a continuous monolayer was formed. The evening before the experiment, the growth medium containing 5% FBS was replaced with growth medium containing 1% FBS. Cells were pretreated with or without 4F (10 μg/ml) for 60 minutes at 37°C (n = 3 in each group). After this, F-Aβ42 was spiked into the media (1.5 μg/ml) and then further incubated for 60 minutes. Cells were washed three times with ice-cold PBS, fixed in 4% paraformaldehyde for 60 minutes on ice, and then mounted with ProLong Diamond mounting media containing 4′,6-diamidino-2-phenylindole (Invitrogen). Cell monolayers were imaged using a Zeiss LSM 780 laser confocal microscope using a C-Apochromat 40×/1.2-W objective.

Statistical Analysis. All statistical tests were conducted using GraphPad Prism (GraphPad software, La Jolla, CA). A P value of $<$ 0.05 was considered statistically significant. One-way ANOVA with Tukey's post-tests were used to compare the [^{125}I]4F versus [^{125}I] ApoA-I distribution in various brain regions. Unpaired, two-tailed t tests were used to compare the [^{125}I]Aβ distribution in the brain or plasma in mice, the [^{125}I]Aβ flux in vitro, and the F-Aβ uptake in vitro in groups with versus without 4F treatment.

Results

Brain Influx of [^{125}I]4F Is Substantially Higher than [^{125}I]ApoA-I. After femoral injection, the permeability of [^{125}I]4F and [^{125}I]ApoA-I at each brain region was determined as the PS product, which was obtained by dividing the total radioactivity per gram tissue by the plasma AUC_{0-t} (Fig. 1A). The [^{125}I]4F permeability at various brain regions ranged from 2 to 5 × 10^{-6} ml/g per second, which was ~1000-fold greater ($P < 0.0001$, one-way ANOVA with Tukey's post-tests) compared with the [^{125}I]ApoA-I permeability, which ranged from 2 to 12 × 10^{-9} ml/g per second at various brain regions (Fig. 1B).

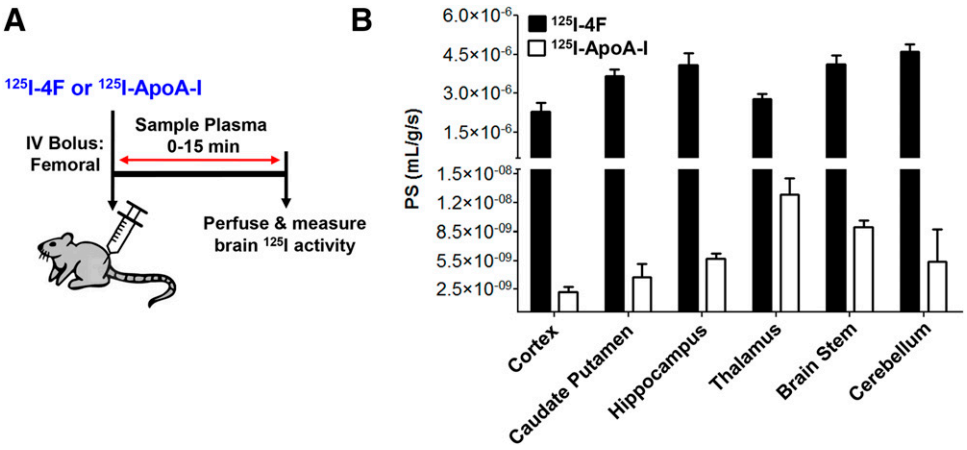

Fig. 1. Brain influx of [^{125}I]4F is substantially higher than [^{125}I]ApoA-I. (A) Experimental scheme. B6SJLF1/J mice were bolus-injected with 100 μCi of [^{125}I]4F or [^{125}I]ApoA-I via the femoral vein. Blood was sampled periodically from the femoral artery from 0 to 15 minutes. The plasma was separated, the intact protein was precipitated with TCA, and the radioactivity was measured. After the final sampling event, mice were transcardially perfused with excess PBS, brain regions were dissected, and the radioactivity was measured. (B) The [^{125}I]4F vs. [^{125}I]ApoA-I PS product estimates are shown for various brain regions. Data represent means ± S.D. (n = 4). ***$P < 0.0001$; one-way ANOVA.

4F Promotes the Brain Efflux of [^{125}I]Aβ42. After infusion with saline or 4F (2 mg) via the internal carotid artery, [^{125}I]Aβ42 (0.7 μCi) was stereotaxically injected into the right hippocampus. After 40 minutes, the ^{125}I radioactivity retained in the brain was measured and normalized to the radioactivity at the site of injection (Fig. 2). In mice infused with 4F, the retention of [^{125}I]Aβ42 in the whole brain (1.7 ± 0.2, means ± S.D., n = 3) was decreased by ~2-fold ($P < 0.05$, two-tailed t test) compared with mice infused with saline control (4.0 ± 1.2, means ± S.D., n = 3). Similar trends were observed for the right hemisphere, in which the [^{125}I]Aβ42 retention was decreased ($P < 0.05$, two-tailed t test) in the 4F-infused mice (1.6 ± 0.2) compared with the saline control (2.9 ± 0.6). The observed decrease in brain retention is reflective of increased brain efflux.

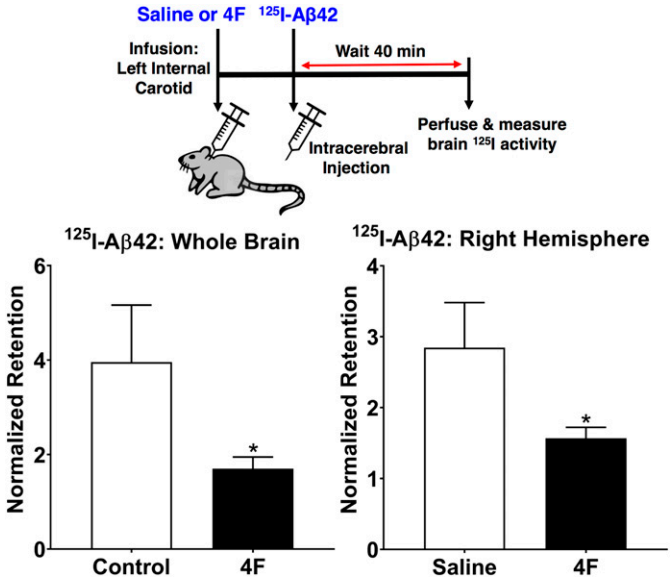

Fig. 2. 4F promotes the brain efflux of [^{125}I]Aβ42. Mice were infused with saline or 4F (2 mg) via the left internal carotid artery over a period of 60 minutes. At the end of infusion, [^{125}I]Aβ42 (0.7 μCi) was stereotaxically injected into the right hippocampus. After 40 minutes, the mice were transcardially perfused with excess PBS, and the radioactivity retained in the whole brain and right hemisphere was measured. The bar charts indicate the radioactivity in whole brain or right hemisphere relative to the radioactivity at the injection site. Data represent means ± S.D. (n = 3). *$P < 0.05$; unpaired two-tailed t test.

4F Inhibits the Brain Influx of [^{125}I]Aβ42 but Not [^{125}I]Aβ40. The influx of [^{125}I]Aβ42 and [^{125}I]Aβ40 into the brain after femoral injection was assessed as the PS product, determined using the methods described above for [^{125}I]4F. In mice infused with 4F, the influx of [^{125}I]Aβ42 into the hippocampus (0.34 ± 0.09 × 10^{-4} ml/g per second, means ± S.D., n = 3) decreased by ~4-fold ($P < 0.0001$, two-tailed t test) compared with mice infused with saline control (1.3 ± 0.2 ml/g per second × 10^{-4}, means ± S.D., n = 3) (Fig. 3A). The hippocampus is the brain region most severely compromised in Alzheimer disease (Smith, 2002). The Aβ influx into the individual brain hemispheres was also evaluated. In mice infused with 4F, the influx of [^{125}I]Aβ42 into the left hemisphere (0.54 ± 0.16 × 10^{-4} ml/g per second) decreased by ~2-fold ($P < 0.05$, two-tailed t test) compared with mice infused with saline control (1.1 ± 0.3 × 10^{-4} ml/g per second) (Fig. 3B). In contrast, a nonsignificant increase (P = 0.13, two-tailed t test) in [^{125}I]Aβ40 influx into the left hemisphere was observed in the 4F-infused mice (1.4 ± 0.8 × 10^{-4} ml/g per second, means ± S.D., n = 3) when compared with saline-infused mice (0.70 ± 0.54 × 10^{-4} ml/g per second, means ± S.D., n = 3) (Fig. 3C).

Impact of 4F on [^{125}I]Aβ42 and [^{125}I]Aβ40 Plasma Pharmacokinetics. The [^{125}I]Aβ42 and [^{125}I]Aβ40 plasma concentration versus time data between 0 and 15 minutes after femoral injection were evaluated by noncompartmental analysis (Fig. 4). The AUC_{0-t} and terminal clearance of [^{125}I]Aβ42 in saline-infused mice were estimated as 25.3 ± 18.4 min × μCi/ml and 4.1 ± 2.3 ml/min (means ± S.D., n = 3), respectively. These parameters were not significantly altered in the 4F-infused mice and were found to be 39.5 ± 27.6 min × μCi/ml (means ± S.D., n = 3) and 2.9 ± 1.6 ml/min, respectively. For [^{125}I]Aβ40, the AUC_{0-t} and terminal clearance in saline-infused mice were estimated as 53.3 ± 11.7 min × μCi/ml and 1.6 ± 0.3 ml/min (means ± S.D., n = 3), respectively. These parameters were unaltered in the 4F-infused mice and were estimated as 49.3 ± 16.2 min × μCi/ml and 1.5 ± 0.5 ml/min (means ± S.D., n = 3), respectively.

4F Promotes the Abluminal-to-Luminal Flux and Inhibits the Luminal-to-Abluminal Flux of [^{125}I]Aβ42 Across BBB Cell Monolayers. To corroborate the in vivo findings, further studies were conducted to examine the transport of [^{125}I]Aβ42 across hCMEC/D3 monolayers cultured on Transwell filters, a widely used in vitro BBB model (Weksler et al., 2013). The [^{125}I]Aβ42 transport was

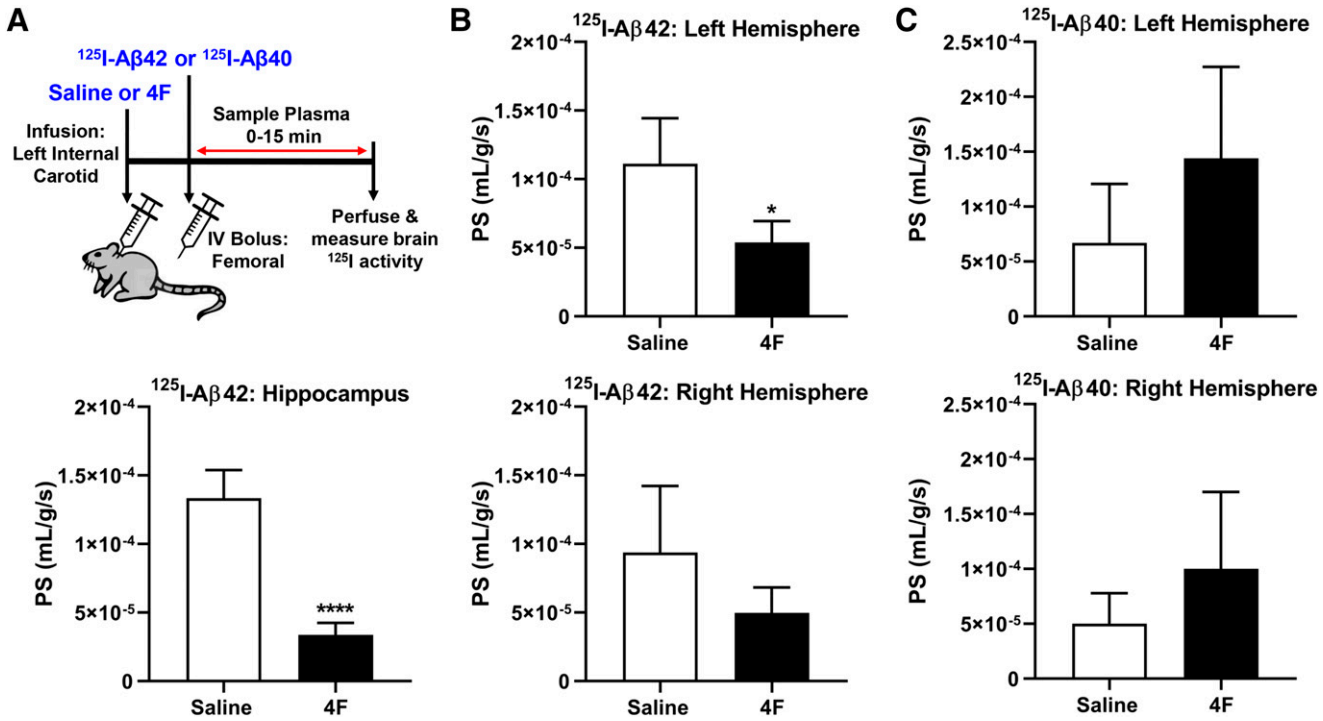

Fig. 3. 4F inhibits the brain influx of [^{125}I]Aβ42 but not [^{125}I]Aβ40. (A) Experimental scheme. Mice were infused with saline or 4F (2 mg) via the left internal carotid artery over a period of 60 minutes. After this, 100 μCi of [^{125}I]Aβ42 or [^{125}I]Aβ40 was bolus-injected via the femoral vein. Blood was sampled periodically from the femoral artery from 0 to 15 minutes. Postperfusion with PBS, the brain regions were harvested, and the radioactivity was measured. (B) The PS product estimates for [^{125}I]Aβ42 in the left/right hemispheres and hippocampus are shown. Data represent means ± S.D. (n = 3). *$P < 0.05$; unpaired two-tailed t test. (C) The PS product estimates for [^{125}I]Aβ40 in the left/right hemispheres are shown. Data represent means ± S.D. (n = 3).****p < 0.001;

investigated in both directions. To study the A-L transport (i.e., from brain to blood), cells were treated with 4F, and then [^{125}I]Aβ42 was added together on the abluminal side, followed by periodic sampling on the luminal side (Fig. 5A). The slope of the linear portion of the cumulative radioactivity versus time plot estimates the [^{125}I]Aβ42 flux in the A-L direction. The A-L flux was increased by ~2-fold ($P < 0.05$, two-tailed t test) in the 4F-treated cells ($4.9 \pm 0.4 \times 10^{-4}$ μCi/min, means ± S.D., n = 4) as compared with the untreated control ($2.8 \pm 0.3 \times 10^{-4}$ μCi/min, means ± S.D., n = 4). To study the L-A transport (i.e., from blood to brain), cells were treated with 4F, and then [^{125}I]Aβ42 was added together on the luminal side, followed by periodic sampling on the abluminal side (Fig. 5B). The [^{125}I]Aβ42 flux in the L-A direction was decreased by ~2-fold ($P < 0.05$, two-tailed t test) in the 4F-treated cells ($2.2 \pm 0.2 \times 10^{-4}$ μCi/min, means ± S.D., n = 4) compared with the untreated control ($4.9 \pm 0.9 \times 10^{-4}$ μCi/min, means ± S.D., n = 4).

4F Inhibits the Accumulation of Fluorescein-Labeled Aβ42 in BBB Cell Monolayers. The effects of 4F on the uptake of fluorescein-labeled Aβ (F-Aβ) in hCMEC/D3 monolayers was further investigated. Treatment with 4F decreased the cellular uptake of F-Aβ42 by ~1.4-fold ($P < 0.05$, two-tailed t test) when assessed by flow cytometry (Fig. 6A). In contrast, no significant differences were observed in the cell

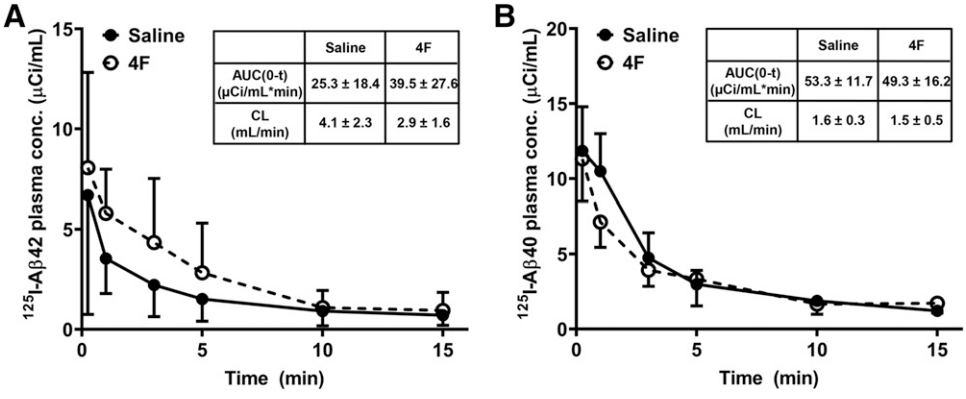

Fig. 4. Impact of 4F on [^{125}I]Aβ42 and [^{125}I]Aβ40 plasma pharmacokinetics. Mice were infused with saline or 4F (2 mg) via the left internal carotid artery over a period of 60 minutes. After this, 100 μCi of [^{125}I]Aβ42 or [^{125}I]Aβ40 was bolus-injected via the femoral vein. Blood was sampled periodically from the femoral artery between 0 and 15 minutes. The plasma was separated, the intact protein was precipitated with TCA, and the radioactivity was measured. The plasma concentration vs. time profiles for [^{125}I]Aβ42 (A) and [^{125}I]Aβ40 (B) were evaluated by noncompartmental analysis. Inset tables show estimates for the area under the concentration vs. time curve from 0 to 15 minutes (AUC_{0-t}) and the terminal clearance (CL). Data represent means ± S.D. (n = 3).

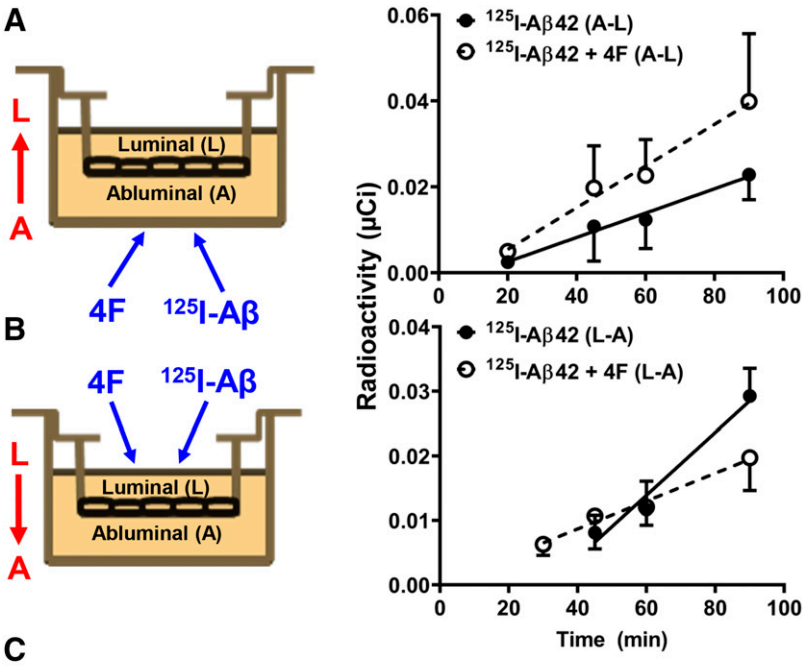

C

	^{125}I-Aβ42	^{125}I-Aβ42 + 4F	Signif.
(A-L) Flux (μCi/min/cm^2 x 10^{-4})	2.5 ± 0.3	4.3 ± 0.4	*
(L-A) Flux (μCi/min/cm^2 x 10^{-4})	4.3 ± 0.8	1.9 ± 0.2	*

Fig. 5. 4F promotes the abluminal-to-luminal flux and inhibits the luminal-to-abluminal flux of [^{125}I]Aβ42 across BBB cell monolayers. Polarized hCMEC/D3 monolayers cultured on Transwell filters were treated with 4F (10 μg/ml) and ^{125}I radiolabeled Aβ42 (10 μCi/ml) together on the abluminal side to investigate A-L flux (A) or on the luminal side to investigate L-A flux (B). The receiver medium was periodically sampled from the contralateral side, and the radioactivity was measured. Cumulative radioactivity was plotted against time, and the linear region was fit to a linear regression model. Data represent means ± S.D. (n = 4). (C) Flux was obtained by dividing the linear regression slope by the surface area (1.12 cm^2) of the insert. Data represent means ± S.E. (n = 4). *$P < 0.05$; unpaired two-tailed t test.

uptake of F-Aβ40 after treatment with 4F (Fig. 6B). Further, confocal micrographs depicted lower intracellular accumulation of F-Aβ42 in cells treated with 4F (Fig. 6C).

Discussion

It is well established that plasma ApoA-I levels are strong predictors of cardiovascular risk. Given that CVD and AD are closely linked, it is likely that decreased serum ApoA-I levels contribute to cerebrovascular dysfunction in AD. This claim is strongly supported by published reports that have demonstrated inverse correlations between plasma ApoA-I levels and AD risk in elderly patients (Saczynski et al., 2007; Ma et al., 2015; Slot et al., 2017). We previously showed that CAA, the most prevalent cerebrovascular pathology in AD, and cognitive decline could be mitigated by increasing ApoA-I levels in the plasma of AD transgenic mice (Lewis et al., 2010). However, the mechanisms by which ApoA-I promotes cerebrovascular Aβ clearance and thereby protects from CAA and related neurovascular pathologies are poorly understood.

Our previous studies have shown that increased Aβ uptake on the luminal side and/or decreased Aβ efflux from the abluminal side could trigger Aβ buildup in the cerebral vasculature (Agyare et al., 2013), which is expected to further impede Aβ clearance from the brain. Hence, it is likely that ApoA-I reduces cerebrovascular Aβ deposition by modulating Aβ trafficking machinery at the BBB. Interestingly, ApoA-I on the luminal side was shown to increase Aβ efflux in the abluminal-to-luminal direction across cerebrovascular endothelial cell monolayers (Merino-Zamorano et al., 2016). However, it remains unclear whether it is ApoA-I in the plasma, in the brain, or both that drive cerebrovascular Aβ clearance.

Decreased ApoA-I levels in the brain and cerebrospinal fluid are associated with neurologic diseases such as schizophrenia (Huang et al., 2008). ApoA-I is majorly produced in the periphery, with little to no production in the brain (Elliott et al., 2010). Thus, the ApoA-I present in brain is thought to be delivered from systemic circulation via trafficking at the BBB endothelium and/or the blood–cerebrospinal fluid barrier epithelium. ApoA-I is a large protein, and its permeability at these barriers is extremely low (Stukas et al., 2014; Zhou et al., 2019). Hence, it is important to consider ApoA-I mimetic peptides, like 4F, as therapeutic alternatives. Further, the 18-amino-acid 4F peptide is more amenable to pharmaceutical development compared with the full-length ApoA-I protein. As a small, amphipathic peptide that interacts with the plasma membrane (Datta et al., 2001), 4F is expected to cross the BBB efficiently. To confirm this in vivo, the PS product, a widely used parameter to assess the brain uptake of macromolecules, was determined after systemic injection of [^{125}I]4F or [^{125}I]ApoA-I in mice. The PS values of [^{125}I]4F at various brain regions were ~1000-fold greater than those determined for [^{125}I]ApoA-I and were commensurate to that of proteins like transferrin and insulin, which are efficiently delivered across the BBB (Poduslo et al., 1994). In contrast, the PS values of [^{125}I]ApoA-I were similar to those of proteins that demonstrate very low BBB permeability, such as immunoglobulin G and albumin (Poduslo et al., 1994). The efficient brain penetrance of 4F provides a plausible mechanistic interpretation of the robust 4F effects on neuropathology in AD mice. Given that PS values are representative only of influx, the impact of 4F brain efflux on the overall brain delivery remains to be clarified.

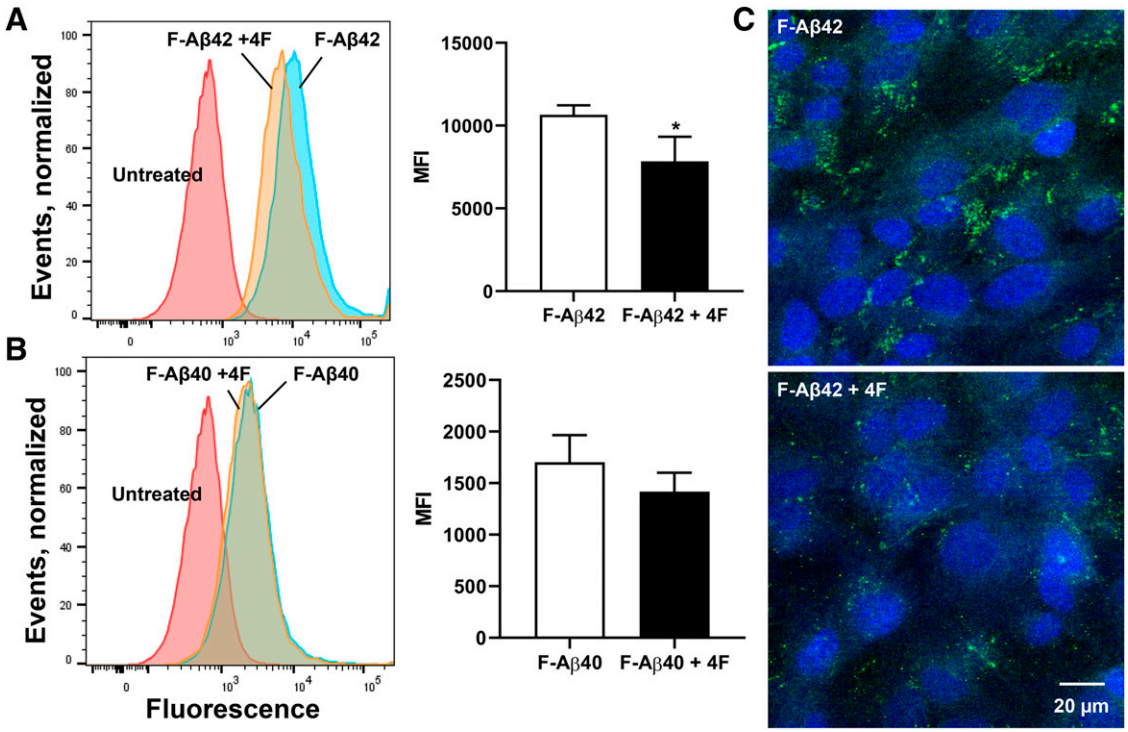

Fig. 6. 4F inhibits the accumulation of fluorescein-labeled Aβ42 in BBB cell monolayers. hCMEC/D3 monolayers were treated for 60 minutes with 10 μg/ml 4F peptide, followed by another 60 minutes with 12.5 μg/ml of fluorescein-labeled Aβ42 (F-Aβ42) (A) or F-Aβ40 (B). The fluorescence uptake was assessed by flow cytometry. Shown are representative histograms and bar charts of the group means ± S.D. ($n = 3$). *$P < 0.05$; unpaired two-tailed t test. (C) Confocal micrographs are shown depicting F-Aβ42 internalization in hCMEC/D3 monolayers cultured on coverslip dishes after 4F treatment as described above (representative images, $n = 3$). Green = F-Aβ42; blue = 4′,6-diamidino-2-phenylindole–stained nuclei.

Further, we investigated the ability of 4F to modulate Aβ trafficking from brain to blood and from blood to brain. To assess 4F's effect on [^{125}I]Aβ42 clearance from brain to blood, the [^{125}I]Aβ42 radioactivity retained in the brain after intracerebral injection was assessed in mice infused with 4F via the internal carotid artery, which supplies blood directly to the brain. This experimental modality allowed us to specifically investigate 4F's effects on [^{125}I]Aβ42 transport at the BBB. The brain retention of [^{125}I]Aβ42 was substantially decreased in 4F-treated mice, which could be attributed to increased [^{125}I]Aβ42 brain efflux. It was also observed that after femoral injection, the brain influx of [^{125}I]Aβ42, assessed as the PS product, was substantially decreased in 4F-treated mice. Together, these findings indicate that 4F reduces the brain accumulation of [^{125}I]Aβ42 by increasing its brain-to-blood efflux and by decreasing its blood-to-brain influx. Intriguingly, 4F exhibited distinct effects in modulating the brain influx of [^{125}I]Aβ40 as compared with [^{125}I]Aβ42; a nonsignificant increase in [^{125}I]Aβ40 brain influx was observed in the 4F-treated mice. Importantly, Aβ42 is considered to be more neurotoxic and amyloidogenic than Aβ40, and parenchymal amyloid plaques in AD brain are seeded by Aβ42 aggregates (Miller et al., 1993). Additionally, Aβ40 is reported to inhibit Aβ42 oligomerization, fibrillogenesis, and toxicity (Jan et al., 2008; Murray et al., 2009). In patients with AD, the accelerated amyloid accumulation in the cerebral vasculature and brain parenchyma is thought to be majorly due to the impaired Aβ42 clearance from brain to blood (Sagare et al., 2012). By helping to restore Aβ42 clearance at the BBB, 4F could thereby reduce both cerebrovascular and parenchymal amyloid burden in AD brain.

No significant differences were observed in the [^{125}I]Aβ42 plasma pharmacokinetics in 4F-treated mice, although a visual trend of increased AUC with a concomitant decrease in terminal clearance was observed. The apparent decrease in plasma clearance of [^{125}I]Aβ42 in the presence of 4F could be due to altered Aβ42 clearance mechanisms in kidneys and liver, which represent the major organs responsible for systemic Aβ clearance (Ghiso et al., 2004). Since the plasma disposition of Aβ and its trafficking at the BBB are thought to be handled by low-density lipoprotein receptor-related protein 1 (LRP1) and scavenger receptor class B type 1 (Martins et al., 2009; Thanopoulou et al., 2010), both of which are highly expressed in the vascular endothelium, we speculate that 4F modulates Aβ disposition by interacting with these receptors. It was previously shown that HDL transcytosis at the BBB is mediated by scavenger receptor class B type 1 (Fung et al., 2017). Furthermore, ATP-binding cassette transporter A1 (ABCA1), expressed on the abluminal surface of the BBB endothelium, was shown to mediate the brain efflux of Aβ42 (Elali and Rivest, 2013). As a major lipid transporter, ABCA1 interacts with HDL/ApoA-I and other apolipoproteins that mediate lipid efflux and reverse cholesterol transport. Studies have shown that ABCA1 overexpression mitigates, whereas ABCA1 deletion exacerbates, brain Aβ deposition in AD mice (Wahrle et al., 2005, 2008). We recently showed that 4F interacts with ABCA1 to mediate cholesterol/lipid efflux (Chernick et al., 2018). Thus, the altered brain influx of [^{125}I]Aβ42 upon 4F treatment could potentially be mediated by effects on ABCA1 at the BBB.

Since only female mice were used in this study, further studies are needed to examine potential sex differences in 4F

efficacy. In various AD transgenic mouse models, such as 3xTg-AD (Carroll et al., 2010; Gali et al., 2019), APP/PS1, and Tg2576 mice (Callahan et al., 2001), female mice were reported to exhibit higher Aβ levels and greater occurrence of histopathological hallmarks compared with their male littermates. Moreover, sex differences were also apparent in the efficacy of experimental AD therapies that mitigate Aβ pathology (Long et al., 2016; Dodiya et al., 2019). In this study, experiments were conducted solely on female mice so that follow-up studies can be pursued in female APP/PS1 mice, which are reported to manifest higher Aβ levels compared with the male mice. The APP/PS1 mice will serve as a more stringent model to test the efficacy and mechanistic action of 4F.

To verify the in vivo findings, we investigated [^{125}I]Aβ42 transcytosis in both directions across BBB cell monolayers cultured on Transwell filters. Treatment with 4F was shown to increase the abluminal-to-luminal flux of [^{125}I]Aβ42, which is consistent with the increased brain efflux of [^{125}I]Aβ42 observed in 4F-treated mice. We further showed that 4F decreased the luminal-to-abluminal flux of [^{125}I]Aβ42, which is consistent with the decreased brain influx of [^{125}I]Aβ42 observed in 4F-treated mice. Together, these findings indicate that 4F differentially modulates [^{125}I]Aβ42 trafficking at the BBB in the luminal-to-abluminal (blood to brain) versus abluminal-to-luminal (brain to blood) directions.

To investigate the effects of 4F on cerebrovascular accumulation of Aβ, which predominates in both CAA and AD, we evaluated the cellular uptake of fluorescein-labeled Aβ in BBB cell monolayers after 4F treatment. When assessed by flow cytometry, the uptake of F-Aβ42 was found to be decreased in 4F-treated cells, whereas the F-Aβ40 uptake was not significantly altered. Using laser confocal microscopy, we also demonstrated lower intracellular accumulation of F-Aβ42 in 4F-treated cells. Although Aβ40 is the predominant isoform present in the cerebrovascular amyloid deposits, Aβ42 was shown to seed the formation of these deposits (Roher et al., 1993; McGowan et al., 2005). Thus, 4F could be effective in reducing cerebrovascular Aβ deposition in CAA and AD.

In summary, the brain permeability of [^{125}I]4F, assessed as the PS product, was found to be ~1000-fold greater than that of [^{125}I]ApoA-I and was comparable to proteins like transferrin and insulin, which rapidly permeate across the BBB. Moreover, systemic infusion of 4F was shown to modulate the BBB trafficking of [^{125}I]Aβ42 by increasing its brain-to-blood efflux and by decreasing its blood-to-brain influx. These findings clarify the effects of 4F on specific Aβ isoforms and provide a mechanistic interpretation of the decreased brain Aβ deposition reported in AD transgenic mice after chronic oral dosing of 4F (Handattu et al., 2009). However, it remains unclear whether 4F elicits these beneficial effects by acting on the luminal side or by acting within the brain parenchyma after crossing the BBB. Further studies are needed to clarify the molecular mechanisms by which 4F alleviates Aβ-associated neuropathologies in CAA and AD. Although clinical efficacy of 4F was demonstrated in patients with CVD (Bloedon et al., 2008; Dunbar et al., 2017), the efficacy of 4F in treating patients with AD remains to be carefully elucidated, especially in the perspective of challenges encountered in the clinical translation of anti-Aβ therapeutics. Nevertheless, as an ApoA-I/HDL mimetic peptide, 4F also possesses antioxidative and inflammatory properties and thus presents a novel therapeutic approach to enhance cerebrovascular function as well as to mitigate brain Aβ accumulation in CAA and AD.

Authorship Contributions

Participated in research design: Swaminathan, Zhou, Ahlschwede, Li, Kandimalla.

Conducted experiments: Swaminathan, Zhou, Ahlschwede, Curran.

Contributed new reagents or analytic tools: Li.

Performed data analysis: Swaminathan, Zhou, Ahlschwede, Kandimalla.

Wrote or contributed to the writing of the manuscript: Swaminathan, Zhou, Lowe, Li, Kandimalla.

References

Agyare EK, Leonard SR, Curran GL, Yu CC, Lowe VJ, Paravastu AK, Poduslo JF, and Kandimalla KK (2013) Traffic jam at the blood-brain barrier promotes greater accumulation of Alzheimer's disease amyloid-β proteins in the cerebral vasculature. *Mol Pharm* **10**:1557–1565.

Anantharamaiah GM, Mishra VK, Garber DW, Datta G, Handattu SP, Palgunachari MN, Chaddha M, Navab M, Reddy ST, Segrest JP, et al. (2007) Structural requirements for antioxidative and anti-inflammatory properties of apolipoprotein A-I mimetic peptides. *J Lipid Res* **48**:1915–1923.

Assmann G and Gotto AM Jr. (2004) HDL cholesterol and protective factors in atherosclerosis. *Circulation* **109** (Suppl 1):III8-III14.

Bloedon LT, Dunbar R, Duffy D, Pinell-Salles P, Norris R, DeGroot BJ, Movva R, Navab M, Fogelman AM, and Rader DJ (2008) Safety, pharmacokinetics, and pharmacodynamics of oral apoA-I mimetic peptide D-4F in high-risk cardiovascular patients. *J Lipid Res* **49**:1344–1352.

Buga GM, Frank JS, Mottino GA, Hendizadeh M, Hakhamian A, Tillisch JH, Reddy ST, Navab M, Anantharamaiah GM, Ignarro LJ, et al. (2006) D-4F decreases brain arteriole inflammation and improves cognitive performance in LDL receptor-null mice on a Western diet. *J Lipid Res* **47**:2148–2160.

Button EB, Robert J, Caffrey TM, Fan J, Zhao W, and Wellington CL (2019) HDL from an Alzheimer's disease perspective. *Curr Opin Lipidol* **30**:224–234.

Callahan MJ, Lipinski WJ, Bian F, Durham RA, Pack A, and Walker LC (2001) Augmented senile plaque load in aged female beta-amyloid precursor protein-transgenic mice. *Am J Pathol* **158**:1173–1177.

Carroll JC, Rosario ER, Kreimer S, Villamagna A, Gentzschein E, Stanczyk FZ, and Pike CJ (2010) Sex differences in β-amyloid accumulation in 3xTg-AD mice: role of neonatal sex steroid hormone exposure. *Brain Res* **1366**:233–245.

Charidimou A, Gang Q, and Werring DJ (2012) Sporadic cerebral amyloid angiopathy revisited: recent insights into pathophysiology and clinical spectrum. *J Neurol Neurosurg Psychiatry* **83**:124–137.

Chernick D, Ortiz-Valle S, Jeong A, Swaminathan SK, Kandimalla KK, Rebeck GW, and Li L (2018) High-density lipoprotein mimetic peptide 4F mitigates amyloid-β-induced inhibition of apolipoprotein E secretion and lipidation in primary astrocytes and microglia. *J Neurochem* **147**:647–662.

Datta G, Chaddha M, Hama S, Navab M, Fogelman AM, Garber DW, Mishra VK, Epand RM, Epand RF, Lund-Katz S, et al. (2001) Effects of increasing hydrophobicity on the physical-chemical and biological properties of a class A amphipathic helical peptide. *J Lipid Res* **42**:1096–1104.

Dodiya HB, Kuntz T, Shaik SM, Baufeld C, Leibowitz J, Zhang X, Gottel N, Zhang X, Butovsky O, Gilbert JA, et al. (2019) Sex-specific effects of microbiome perturbations on cerebral Aβ amyloidosis and microglia phenotypes. *J Exp Med* **216**:1542–1560.

Dunbar RL, Movva R, Bloedon LT, Duffy D, Norris RB, Navab M, Fogelman AM, and Rader DJ (2017) Oral apolipoprotein A-I mimetic D-4F lowers HDL-inflammatory index in high-risk patients: a first-in-human multiple-dose, randomized controlled trial. *Clin Transl Sci* **10**:455–469.

Elali A and Rivest S (2013) The role of ABCB1 and ABCA1 in beta-amyloid clearance at the neurovascular unit in Alzheimer's disease. *Front Physiol* **4**:45.

Elliott DA, Weickert CS, and Garner B (2010) Apolipoproteins in the brain: implications for neurological and psychiatric disorders. *Clin Lipidol* **51**:555–573.

Fagan AM, Christopher E, Taylor JW, Parsadanian M, Spinner M, Watson M, Fryer JD, Wahrle S, Bales KR, Paul SM, et al. (2004) ApoAI deficiency results in marked reductions in plasma cholesterol but no alterations in amyloid-beta pathology in a mouse model of Alzheimer's disease-like cerebral amyloidosis. *Am J Pathol* **165**:1413–1422.

Fung KY, Wang C, Nyegaard S, Heit B, Fairn GD, and Lee WL (2017) SR-BI mediated transcytosis of HDL in brain microvascular endothelial cells is independent of caveolin, clathrin, and PDZK1. *Front Physiol* **8**:841.

Gali CC, Fanaee-Danesh E, Zandl-Lang M, Albrecher NM, Tam-Amersdorfer C, Stracke A, Sachdev V, Reichmann F, Sun Y, Avdili A, et al. (2019) Amyloid-beta impairs insulin signaling by accelerating autophagy-lysosomal degradation of LRP-1 and IR-β in blood-brain barrier endothelial cells in vitro and in 3XTg-AD mice. *Mol Cell Neurosci* **99**:103390.

Ghiso J, Shayo M, Calero M, Ng D, Tomidokoro Y, Gandy S, Rostagno A, and Frangione B (2004) Systemic catabolism of Alzheimer's Abeta40 and Abeta42. *J Biol Chem* **279**:45897–45908.

Handattu SP, Garber DW, Monroe CE, van Groen T, Kadish I, Nayyar G, Cao D, Palgunachari MN, Li L, and Anantharamaiah GM (2009) Oral apolipoprotein A-I mimetic peptide improves cognitive function and reduces amyloid burden in a mouse model of Alzheimer's disease. *Neurobiol Dis* **34**:525–534.

Herzig MC, Van Nostrand WE, and Jucker M (2006) Mechanism of cerebral beta-amyloid angiopathy: murine and cellular models. *Brain Pathol* **16**:40–54.
Hottman DA, Chernick D, Cheng S, Wang Z, and Li L (2014) HDL and cognition in neurodegenerative disorders. *Neurobiol Dis* **72**:22–36.
Huang JT, Wang L, Prabakaran S, Wengenroth M, Lockstone HE, Koethe D, Gerth CW, Gross S, Schreiber D, Lilley K, et al. (2008) Independent protein-profiling studies show a decrease in apolipoprotein A1 levels in schizophrenia CSF, brain and peripheral tissues. *Mol Psychiatry* **13**:1118–1128.
Jan A, Gokce O, Luthi-Carter R, and Lashuel HA (2008) The ratio of monomeric to aggregated forms of Abeta40 and Abeta42 is an important determinant of amyloid-beta aggregation, fibrillogenesis, and toxicity. *J Biol Chem* **283**:28176–28189.
Jaruszewski KM, Curran GL, Swaminathan SK, Rosenberg JT, Grant SC, Ramakrishnan S, Lowe VJ, Poduslo JF, and Kandimalla KK (2014) Multimodal nanoprobes to target cerebrovascular amyloid in Alzheimer's disease brain. *Biomaterials* **35**:1967–1976.
Kandimalla KK, Wengenack TM, Curran GL, Gilles EJ, and Poduslo JF (2007) Pharmacokinetics and amyloid plaque targeting ability of a novel peptide-based magnetic resonance contrast agent in wild-type and Alzheimer's disease transgenic mice. *J Pharmacol Exp Ther* **322**:541–549.
Lefterov I, Fitz NF, Cronican AA, Fogg A, Lefterov P, Kodali R, Wetzel R, and Koldamova R (2010) Apolipoprotein A-I deficiency increases cerebral amyloid angiopathy and cognitive deficits in APP/PS1DeltaE9 mice. *J Biol Chem* **285**: 36945–36957.
Lewis TL, Cao D, Lu H, Mans RA, Su YR, Jungbauer L, Linton MF, Fazio S, LaDu MJ, and Li L (2010) Overexpression of human apolipoprotein A-I preserves cognitive function and attenuates neuroinflammation and cerebral amyloid angiopathy in a mouse model of Alzheimer disease. *J Biol Chem* **285**:36958–36968.
Long Z, Zeng Q, Wang K, Sharma A, and He G (2016) Gender difference in valproic acid-induced neuroprotective effects on APP/PS1 double transgenic mice modeling Alzheimer's disease. *Acta Biochim Biophys Sin (Shanghai)* **48**:930–938.
Ma C, Li J, Bao Z, Ruan Q, and Yu Z (2015) Serum levels of ApoA1 and ApoA2 are associated with cognitive status in older men. *BioMed Res Int* **2015**:481621.
Martins IJ, Berger T, Sharman MJ, Verdile G, Fuller SJ, and Martins RN (2009) Cholesterol metabolism and transport in the pathogenesis of Alzheimer's disease. *J Neurochem* **111**:1275–1308.
McGowan E, Pickford F, Kim J, Onstead L, Eriksen J, Yu C, Skipper L, Murphy MP, Beard J, Das P, et al. (2005) Abeta42 is essential for parenchymal and vascular amyloid deposition in mice. *Neuron* **47**:191–199.
Merino-Zamorano C, Fernández-de Retana S, Montañola A, Batlle A, Saint-Pol J, Mysiorek C, Gosselet F, Montaner J, and Hernández-Guillamon M (2016) Modulation of amyloid-β1-40 transport by ApoA1 and ApoJ across an in vitro model of the blood-brain barrier. *J Alzheimers Dis* **53**:677–691.
Michaud JP, Bellavance MA, Préfontaine P, and Rivest S (2013a) Real-time in vivo imaging reveals the ability of monocytes to clear vascular amyloid beta. *Cell Rep* **5**: 646–653.
Michaud JP, Hallé M, Lampron A, Thériault P, Préfontaine P, Filali M, Tribout-Jover P, Lanteigne AM, Jodoin R, Cluff C, et al. (2013b) Toll-like receptor 4 stimulation with the detoxified ligand monophosphoryl lipid A improves Alzheimer's disease-related pathology. *Proc Natl Acad Sci USA* **110**:1941–1946.
Miller DL, Papayannopoulos IA, Styles J, Bobin SA, Lin YY, Biemann K, and Iqbal K (1993) Peptide compositions of the cerebrovascular and senile plaque core amyloid deposits of Alzheimer's disease. *Arch Biochem Biophys* **301**:41–52.
Morgantini C, Imaizumi S, Grijalva V, Navab M, Fogelman AM, and Reddy ST (2010) Apolipoprotein A-I mimetic peptides prevent atherosclerosis development and reduce plaque inflammation in a murine model of diabetes. *Diabetes* **59**:3223–3228.
Murray MM, Bernstein SL, Nyugen V, Condron MM, Teplow DB, and Bowers MT (2009) Amyloid beta protein: abeta40 inhibits Abeta42 oligomerization. *J Am Chem Soc* **131**:6316–6317.
Navab M, Shechter I, Anantharamaiah GM, Reddy ST, Van Lenten BJ, and Fogelman AM (2010) Structure and function of HDL mimetics. *Arterioscler Thromb Vasc Biol* **30**:164–168.
Poduslo JF, Curran GL, and Berg CT (1994) Macromolecular permeability across the blood-nerve and blood-brain barriers. *Proc Natl Acad Sci USA* **91**: 5705–5709.
Poduslo JF, Curran GL, Wengenack TM, Malester B, and Duff K (2001) Permeability of proteins at the blood-brain barrier in the normal adult mouse and double transgenic mouse model of Alzheimer's disease. *Neurobiol Dis* **8**:555–567.
Qi XM and Ma JF (2017) The role of amyloid beta clearance in cerebral amyloid angiopathy: more potential therapeutic targets. *Transl Neurodegener* **6**:22.
Roher AE, Lowenson JD, Clarke S, Woods AS, Cotter RJ, Gowing E, and Ball MJ (1993) beta-Amyloid-(1-42) is a major component of cerebrovascular amyloid deposits: implications for the pathology of Alzheimer disease. *Proc Natl Acad Sci USA* **90**:10836–10840.
Saczynski JS, White L, Peila RL, Rodriguez BL, and Launer LJ (2007) The relation between apolipoprotein A-I and dementia: the Honolulu-Asia aging study. *Am J Epidemiol* **165**:985–992.
Sagare AP, Bell RD, and Zlokovic BV (2012) Neurovascular dysfunction and faulty amyloid β-peptide clearance in Alzheimer disease. *Cold Spring Harb Perspect Med* **2**:a011452.
Slot RE, Van Harten AC, Kester MI, Jongbloed W, Bouwman FH, Teunissen CE, Scheltens P, Veerhuis R, and van der Flier WM (2017) Apolipoprotein A1 in cerebrospinal fluid and plasma and progression to Alzheimer's disease in non-demented elderly. *J Alzheimers Dis* **56**:687–697.
Smith AD (2002) Imaging the progression of Alzheimer pathology through the brain. *Proc Natl Acad Sci USA* **99**:4135–4137.
Stukas S, Robert J, Lee M, Kulic I, Carr M, Tourigny K, Fan J, Namjoshi D, Lemke K, DeValle N, et al. (2014) Intravenously injected human apolipoprotein A-I rapidly enters the central nervous system via the choroid plexus. *J Am Heart Assoc* **3**: e001156.
Swaminathan SK, Ahlschwede KM, Sarma V, Curran GL, Omtri RS, Decklever T, Lowe VJ, Poduslo JF, and Kandimalla KK (2018) Insulin differentially affects the distribution kinetics of amyloid beta 40 and 42 in plasma and brain. *J Cereb Blood Flow Metab* **38**:904–918.
Thanopoulou K, Fragkouli A, Stylianopoulou F, and Georgopoulos S (2010) Scavenger receptor class B type I (SR-BI) regulates perivascular macrophages and modifies amyloid pathology in an Alzheimer mouse model. *Proc Natl Acad Sci USA* **107**:20816–20821.
Viswanathan A and Greenberg SM (2011) Cerebral amyloid angiopathy in the elderly. *Ann Neurol* **70**:871–880.
Wahrle SE, Jiang H, Parsadanian M, Hartman RE, Bales KR, Paul SM, and Holtzman DM (2005) Deletion of Abca1 increases Abeta deposition in the PDAPP transgenic mouse model of Alzheimer disease. *J Biol Chem* **280**: 43236–43242.
Wahrle SE, Jiang H, Parsadanian M, Kim J, Li A, Knoten A, Jain S, Hirsch-Reinshagen V, Wellington CL, Bales KR, et al. (2008) Overexpression of ABCA1 reduces amyloid deposition in the PDAPP mouse model of Alzheimer disease. *J Clin Invest* **118**:671–682.
Weksler B, Romero IA, and Couraud PO (2013) The hCMEC/D3 cell line as a model of the human blood brain barrier. *Fluids Barriers CNS* **10**:16.
Yamada M and Naiki H (2012) Cerebral amyloid angiopathy. *Prog Mol Biol Transl Sci* **107**:41–78.
Zhou AL, Swaminathan SK, Curran GL, Poduslo JF, Lowe VJ, Li L, and Kandimalla KK (2019) Apolipoprotein A-I crosses the blood-brain barrier through clathrin-independent and cholesterol-mediated endocytosis. *J Pharmacol Exp Ther* **369**: 481–488.

Address correspondence to: Dr. Karunya K. Kandimalla, Department of Pharmaceutics, Brain Barriers Research Center, University of Minnesota College of Pharmacy, 9-149A, Weaver-Densford Hall, 308 Harvard St. SE, Minneapolis, MN 55455. E-mail: kkandima@umn.edu